Excited state g factors in ^{125}Te

S. K. Chamoli,* A. E. Stuchbery, and M. C. East

Department of Nuclear Physics, Research School of Physics and Engineering, Australian National University, Canberra ACT 0200, Australia

(Received 2 July 2009; revised manuscript received 23 September 2009; published 3 November 2009)

The transient-field technique has been used to measure, with considerably improved precision, the g factors of the $3/2^+$ and $5/2^+$ states in ^{125}Te at 444 and 463 keV, respectively, relative to the g factor of the first excited state in ^{126}Te. Together with shell model and weak-coupling core-excitation model calculations, the g-factor measurements provide insight into the orbital occupation of the odd neutron for the low-excitation states in ^{125}Te. A new $9/2^+$ level at 1029 keV, together with a firm $7/2^+$ spin assignment for the level at 1018 keV, identifies candidate states for the coupling of the $s_{1/2}$ neutron to the 4^+ core excitation.

DOI: 10.1103/PhysRevC.80.054301 PACS number(s): 21.10.Ky, 27.60.+j, 23.20.En, 23.20.Gq

I. INTRODUCTION

The availability of radioactive ion beams has made it possible to Coulomb excite neutron-rich Te isotopes [1,2] near ^{132}Sn. An anomalously low value reported for $B(E2; 0_1^+ \rightarrow 2_1^+)$ in $^{136}_{52}\mathrm{Te}_{84}$ [1] has attracted much theoretical attention [3–5]. The small $B(E2)$ value was interpreted [1] as evidence for a predominantly neutron excitation, which is a suggestion supported by some theories [3,4] but not by others [5]. Evidently, there are still uncertainties as to the correct shell model interaction for neutron-rich nuclei beyond ^{132}Sn.

For these reasons, a g-factor measurement on ^{136}Te would prove most enlightening. The feasibility of such a measurement was demonstrated recently by the work of Stone and coworkers [6], who used the recoil in vacuum (RIV) technique to measure the g factor of the first excited state of ^{132}Te produced as a radioactive beam. One problem that must be resolved before this technique can be applied with confidence to ^{136}Te concerns the calibration of the RIV hyperfine interaction. The mean lives of the 2_1^+ states in the stable isotopes ^{122}Te, ^{126}Te, and ^{130}Te, which have been used to calibrate the RIV interaction to date [6,7], are all <12 ps. These lifetimes are significantly shorter than that of the 2_1^+ state in ^{136}Te, which is $\tau = 41 \pm 6$ ps [1,8]. A calibration of the free-ion hyperfine interactions based on the 444-keV $3/2_2^+$ and 463-keV $5/2_1^+$ states in ^{125}Te, which have $\tau = 27$ ps and $\tau = 19$ ps [9], respectively, would overcome this problem.

The structure of ^{125}Te is of interest because it lies near the line where truncated shell model calculations can be compared with models that couple the odd nucleon to a collective core. The challenge for simple weak-coupling core-excitation models of the positive-parity states in ^{125}Te is that the neutron $d_{3/2}$ and $s_{1/2}$ orbits are both close to the Fermi surface.

The g factors of the $3/2_2^+$ and $5/2_1^+$ states in ^{125}Te have been measured previously [10,11], but the precision is limited. Also, the consistency between the precession angles observed for the two transitions depopulating each of these states is poor in both previous measurements probably because of their limited precision. In the present work, we report new results for these g factors, which were measured simultaneously relative to the g factor of the first excited state in ^{126}Te. Because we have performed a new Coulomb excitation measurement with a heavier beam than used in previous studies, new information was also obtained on the low-excitation spectroscopy of ^{125}Te. The structure of low-lying positive-parity states is examined by comparing the experimental g factors with shell model and weak-coupling core-excitation model calculations.

II. EXPERIMENTAL PROCEDURES

Figure 1 is a partial level scheme of ^{125}Te that shows the states most strongly Coulomb excited in the present study and the γ-ray transitions most relevant for the g-factor measurement. Gyromagnetic ratios of the $3/2_2^+$ and $5/2_1^+$ states at 444- and 463-keV excitation energy in ^{125}Te were measured simultaneously, relative to that of the 2_1^+ state in ^{126}Te, by the transient-field technique. Experimental procedures were similar to those in previous work [11–14].

States of interest were Coulomb excited using beams of 195-MeV ^{58}Ni from the Australian National University 14UD Pelletron accelerator. Two runs were performed. In the first run, the target (hereafter called "target I") was composed of 92.8% enriched ^{125}Te, 0.65 mg/cm^2 thick, evaporated onto an annealed iron foil 4.6 mg/cm^2 thick. The supplier's assay gave the isotopic composition of the target as follows: ^{122}Te (0.02%), ^{123}Te (0.04%), ^{124}Te (0.74%), ^{126}Te (4.76%), ^{128}Te (1.08%), and ^{130}Te (0.56%). Tellurium nuclei recoiled through the iron foil, where they experienced the transient field, and stopped in a nonmagnetic backing layer that consisted of an annealed copper foil, approximately 11 mg/cm^2 thick, pressed onto the back of the iron foil using an evaporated layer of 2.8 mg/cm^2 thick indium as adhesive.

The Te layer of the target contained 4.76% ^{126}Te, which provides a reference for the relative g-factor measurements. However, at this level, the statistical precision was not adequate. Therefore, a second run was performed with an additional 0.24 mg/cm^2 of enriched ^{126}Te evaporated onto the front (beam-facing side) of target I. Hereafter the target with additional ^{126}Te is called "target II."

*Present address: Department of Physics, Birla Institute of Technology and Science, Pilani, Rajasthan, India.

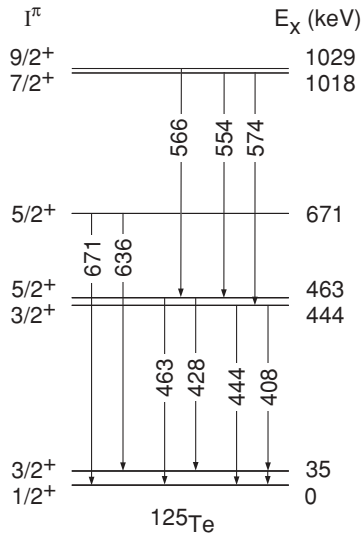

FIG. 1. Partial level scheme of ^{125}Te indicating the levels most strongly Coulomb excited and the γ-ray transitions relevant for the g-factor measurement.

In both runs, the target was mounted in the ANU Hyperfine Spectrometer [15] and maintained at ≈6 K to reduce the effects of beam heating and to help prevent the loss of Te (which has a melting point of 450°C) from the target. This cooling proved effective as no loss of target material was evident throughout the measurements. The iron foils were polarized perpendicular to the γ-ray detection plane by a small electromagnet producing a field of 0.09 T, which is more than sufficient to saturate a well-annealed iron foil [16]. The direction of the polarizing field was reversed automatically, approximately every 15 min.

Backscattered beam ions were detected in a pair of silicon photodiode detectors, 10.1 mm high by 9.2 mm wide, placed 3.83 mm from the beam axis in the vertical plane parallel to the target 16.2 mm upstream of the target; the average scattering angle was 151°. To observe the transient-field precession, γ rays emitted in coincidence with backscattered particles were observed in two 50% (relative efficiency) high-purity germanium (HPGe) detectors and two 20% HPGe detectors placed at forward and backward angles to the beam axis, θ_γ^F and θ_γ^B, respectively, as summarized in Table I. The target-detector distances were set so that the detector crystals all subtended a half-angle of 18°. The γ-ray detectors were placed at various combinations of angles to the beam axis, as shown in Table I, to measure the angular correlations and the transient-field precessions.

Particle-γ coincidence data were recorded in the event-by-event mode with a trigger condition that required a γ-ray to be registered in any of the four HPGe detectors within 800 ns of a backscattered beam ion being recorded in either particle detector. Time differences were recorded for all particle-γ combinations. Although our primary interest is in the particle-γ correlations, the data contain particle-$\gamma\gamma$ coincidences that can be scrutinized to study the level scheme.

TABLE I. Summary of measurements. θ_γ^F and θ_γ^B indicate the angles at which the forward and backward pairs of γ-ray detectors are placed.

Target	θ_γ^F	θ_γ^B	Measurement[a]	Duration (h)
I	±65°	±115°	ϵ, $W(\theta)$	8
I	±60°	±120°	ϵ, $W(\theta)$	20
I	±35°	±120°	ϵ, $W(\theta)$	9
I	±45°	±120°	ϵ, $W(\theta)$	6
I	±55°	±120°	ϵ, $W(\theta)$	9
I	±65°	±120°	ϵ, $W(\theta)$	9
I	0°, −65°	±120°	ϵ, $W(\theta)$	3
I	65°, 0°	±120°	ϵ, $W(\theta)$	3
II	±65°	±115°	ϵ	39
II	±35°	±115°	ϵ	31
II	±60°	±120°	ϵ	24

[a] ϵ: transient-field precession; $W(\theta)$: angular correlation.

III. EXPERIMENTAL RESULTS

A. Level scheme and angular correlations

Figure 2 shows an example of a γ-ray spectrum from target I observed at 60° to the beam in coincidence with backscattered ^{58}Ni ions. Table II lists the lines observed and provides an indication of their intensity relative to the 444-keV transition. For the stronger lines, the intensities were determined from the analysis of the angular correlations. For the weaker lines, the relative intensities were obtained by summing the data for the forward detectors in all measurements with target I, which largely cancels out angular correlation effects. A comparison of this procedure for the stronger lines with the rigorous analysis based on fits to the angular correlations indicates that angular correlation effects can change the relative intensities by no more than 6% in the summed spectrum. All stronger lines in the present work have been identified previously [9] with the exception of the 566-keV transition, which will be discussed later in this article.

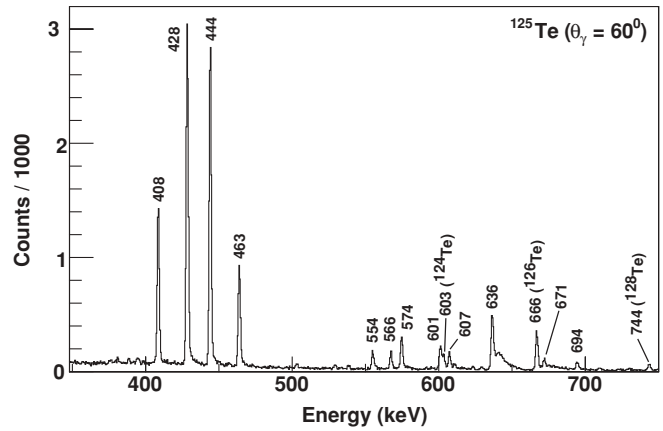

FIG. 2. A γ-ray spectrum observed at +60° to the beam axis in coincidence with backscattered ^{58}Ni. Lines of interest are labeled by their energy. This spectrum represents about half of the data for the field up direction taken with target I (second entry in Table I).

TABLE II. Observed γ-ray intensities after Coulomb excitation of ^{125}Te with 195-MeV ^{58}Ni beams.

E_γ (keV)	I_γ	E_x (keV)	I_i^π	I_f^π
176.3	2.0(1)	321.1	$9/2^-$	$11/2^-$
321.0	0.7(2)	642.2	$7/2^+$	$9/2^-$
346.3	0.9(2)	1017.7	$7/2^+$	$5/2^+$
380.4	1.1(1)	525.2	$7/2^-$	$11/2^-$
388	0.6(1)	not placed[a]		
394.6	1.5(1)	1066.5	$3, 5/2^+$	$5/2^+$
408.1	60(1)	443.6	$3/2^+$	$3/2^+$
427.9	99(1)	463.4	$5/2^+$	$3/2^+$
443.6	100(1)	443.6	$3/2^+$	$1/2^+$
463.4	36(1)	463.4	$5/2^+$	$1/2^+$
503.1	0.8(1)	538.4	$(1/2^+)$	$3/2^+$
528.6	1.2(1)	1066.5	$3, 5/2^+$	$(1/2^+)$
538.4	1.4(1)	538.4	$(1/2^+)$	$1/2^+$
554.4	6.2(1)	1017.7	$7/2^+$	$5/2^+$
566.0	6.7(1)	1029.3	$9/2^+$	$5/2^+$
574.2	15.4(2)	1017.7	$7/2^+$	$3/2^+$
590.4	0.7(1)	1053.9	$3, 5/2^+$	$5/2^+$
600.6	10.4(4)	636.1	$7/2^+$	$3/2^+$
602.7[b]	6(1)		(^{124}Te $2^+ \rightarrow 0^+$)	
603.4[b]	~0.8	1066.5	$3, 5/2^+$	$5/2^+$
606.7	6.1(2)	642.2	$7/2^+$	$3/2^+$
610.2	1.8(2)	1053.9	$3, 5/2^+$	$3/2^+$
622.9	1.2(1)	1066.5	$3, 5/2^+$	$3/2^+$
629	1.2(1)	not placed[c]		
636	56.9(6)	671.4	$5/2^+$	$3/2^+$
666.3	17.9(5)		(^{126}Te $2^+ \rightarrow 0^+$)	
671.4	13(1)	671.4	$5/2^+$	$1/2^+$
693.8	4.6(1)	729.3	$3/2^+$	$3/2^+$
709	0.7(1)	not placed		
722	0.4(2)	not placed[a]		
729.3	1.0(2)	729.3	$3/2^+$	$1/2^+$
743.3	3.1(1)		(^{128}Te $2^+ \rightarrow 0^+$)	
755	0.9(1)	not placed		
772	1.0(2)	not placed[c]		
839.5	1.0(1)		(^{130}Te $2^+ \rightarrow 0^+$)	
885	0.8(1)	not placed[c]		
1018.4	0.7(2)	1053.9	$3, 5/2^+$	$3/2^+$
1030	1.8(2)	not placed[c]		
1066.5	0.8(1)	1066.5	$3, 5/2^+$	$1/2^+$
1097.6	0.4(1)	1133.3	$3, 5/2^+$	$3/2^+$

[a]A line consistent with this energy has been reported previously but not placed [9].
[b]These transitions were not resolved. The total intensity is 6.9(4).
[c]A line consistent with this energy has been placed in ^{125}Te before; however, this observed line is unlikely to be that previously assigned because the excitation energy is too high or lines associated with the previous assignment are not observed.

Branching ratios derived from the data in Table II are in satisfactory agreement with results from previous work. It may be noted that despite the weak population of the 538.4-keV $(1/2^+)$ level, we confirm the branching ratios obtained from the neutron capture study [17] but fail to reproduce the values from β decay adopted in Ref. [9].

TABLE III. $E2/M1$ mixing ratios (δ) in ^{125}Te.

E_γ (keV)	Transition	Mixing ratio (δ)		
		Previous [9]	Present	Adopted
408	$3/2^+ \rightarrow 3/2^+$	+1.50(7)	+1.35(19)	+1.48(7)
444	$3/2^+ \rightarrow 1/2^+$	−2.3(1)	−2.55(14)	−2.38(8)
428	$5/2^+ \rightarrow 3/2^+$	−0.538(11)	−0.48(4)	−0.534(11)
554	$7/2^+ \rightarrow 5/2^+$		−0.14(4)	−0.14(4)
636	$5/2^+ \rightarrow 3/2^+$	+0.332(3)	+0.32(2)	+0.332(3)
694	$3/2^+ \rightarrow 3/2^+$		$+0.34^{+0.17}_{-0.11}$	$+0.34^{+0.17}_{-0.11}$

The measured angular correlations for the stronger lines are compared with the calculated angular correlations in Figs. 3 and 4. Several transitions of interest for the g-factor measurement (408, 444, 428, and 636 keV) have mixed multipolarity. In addition, the 554-, 566-, 574-, and 694-keV transitions were sufficiently strong to determine their multipolarities or mixing ratios for the first time. The mixing ratios were determined from the measured angular correlations by procedures similar to those described in Refs. [18] and [19]. Results are summarized and compared with those of previous work [9] in Table III. The present and previous values, where available, agree very well; weighted average values shown in the final column of Table III were therefore adopted for the analysis of the transient-field precession measurements. The calculated angular correlations in Fig. 3 also correspond to the adopted mixing ratios.

Although the weaker lines are not important for the g-factor measurements, their origin is noted in Table II. Many of these transitions bypass the states for which the g factors are being measured. However, the transitions at 574 and 554 keV are associated with the decay of the 1017.7-keV level in ^{125}Te, which has been identified in neutron capture studies [9] and which decays to the states at 444, 463, and 671 keV. The angular correlation of the 574-keV transition is consistent only with stretched $E2$ multipolarity, and the spin of the 1017.7-keV level (hereafter designated 1018 keV) must be $7/2^+$. As shown in Fig. 3(f), the 566-keV transition is also a stretched $E2$ transition. This transition had not been placed in ^{125}Te; however, its intensity in our measurement, together with its $E2$ character and the fact that it was not observed in previous studies, which have tended to favor the population of lower spin states, suggested that it may be the $9/2^+_1 \rightarrow 5/2^+_1$ transition. This assignment is supported by the particle-$\gamma\gamma$ coincidence data shown in Fig. 5. A gate on the 444-keV transition shows the 574-keV line, whereas a gate on the 428-keV transition clearly shows both the 554- and 566-keV lines, which establishes that both feed into the 463-keV level.

In principle, $B(E2)$ values, and hence level lifetimes, can be gleaned from the relative Coulomb excitation cross sections. The present measurements, however, do not include sufficient information to determine all $E2$ matrix elements needed for a rigorous analysis. With this caveat, we note that observed cross sections suggest $\tau \sim 13 \pm 3$ ps for the 1018-keV $7/2^+$ level and $\tau \sim 33 \pm 6$ ps for the 1029-keV $9/2^+$ level, which is consistent with the absence of Doppler tails on the 554-, 566-, and 574-keV lines.

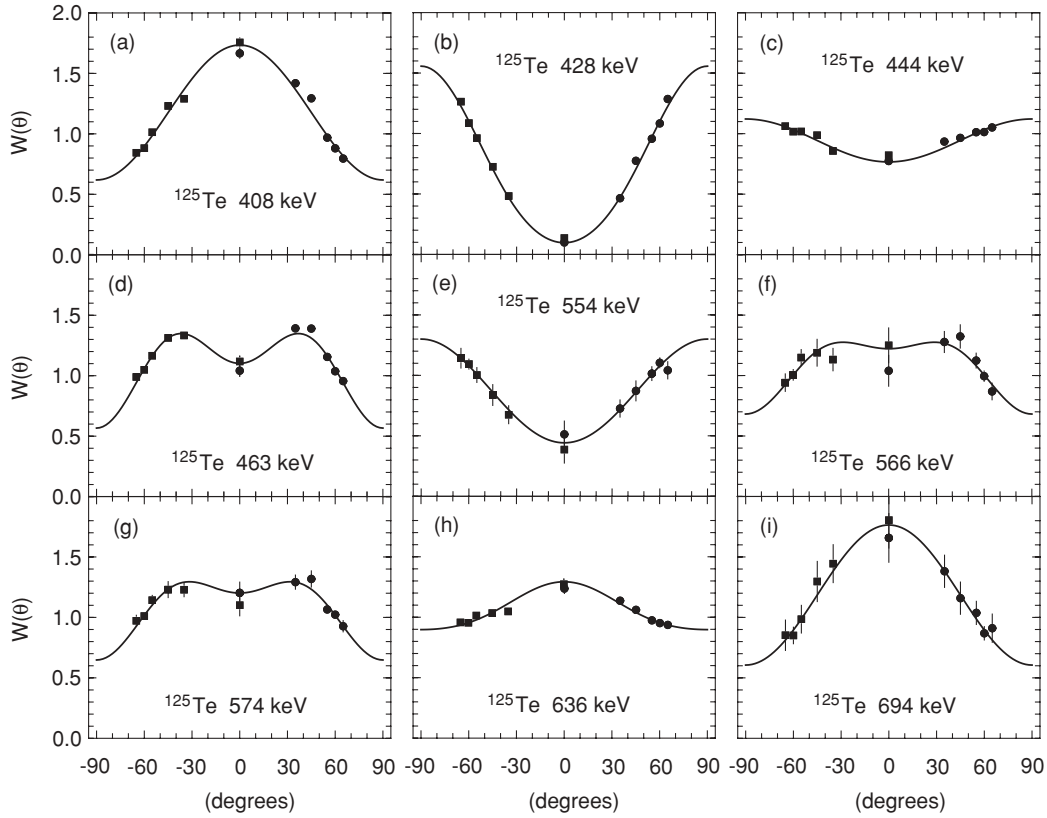

FIG. 3. Measured and calculated angular correlations in ^{125}Te. For the mixed-multipolarity transitions (408, 428, 444, 554, 636, and 694 keV), the calculations use the mixing ratios listed in the last column of Table III.

B. Transient-field g-factor measurement

The transient-field precession angles $\Delta\theta$ were determined by the usual procedures [12,14,20,21]. Briefly, $\Delta\theta = \epsilon/S$, where ϵ is the "effect" and $S(\theta_\gamma) = (1/W)dW/d\theta$ is the logarithmic derivative of the angular correlation at the γ-ray detection angle θ_γ; S is often referred to as the "slope." Formally, $\epsilon = (N\downarrow - N\uparrow)/(N\downarrow + N\uparrow)$, where $N\uparrow(\downarrow)$ refers to the counts recorded for field up (down) at $+\theta_\gamma$; however, the evaluation of ϵ from the experimental data proceeds via the formation of a double ratio of counts recorded for field up and down in a pair of detectors at $\pm\theta_\gamma$.

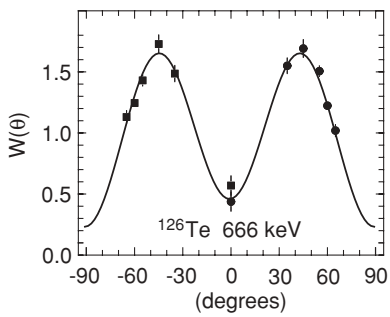

FIG. 4. Measured and calculated angular correlation for the $2_1^+ \rightarrow 0_1^+$ transition in ^{126}Te.

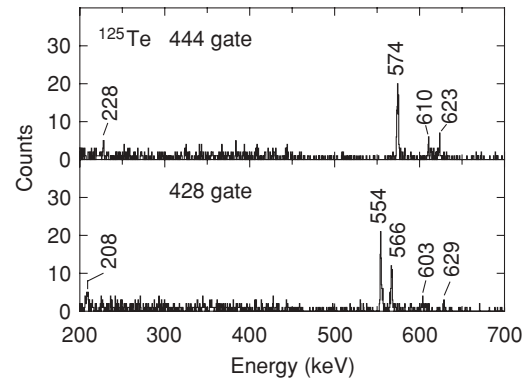

FIG. 5. Spectra projected from the particle-$\gamma\gamma$ data with transitions that feed the $3/2^+$ 444-keV level (upper panel) and the $5/2^+$ 463-keV level (lower panel). The lines at 208 and 228 keV are weak branches from the 671-keV $5/2^+$ level [9] that were not visible in the particle-γ data.

TABLE IV. Slopes of the angular correlations for transitions in ^{125}Te.

E_γ (keV)	Transition	$S(35°)$	$S(45°)$	$S(55°)$	$S(60°)$	$S(65°)$
408	$3/2^+ \rightarrow 3/2^+$	−0.77	−0.95	−1.07	−1.08	−1.04
444	$3/2^+ \rightarrow 1/2^+$	+0.38	+0.38	+0.33	+0.30	+0.26
428	$5/2^+ \rightarrow 3/2^+$	+2.62	+2.09	+1.58	+1.34	+1.11
463	$5/2^+ \rightarrow 1/2^+$	+0.09	−0.42	−0.99	−1.26	−1.48

TABLE V. Transient-field precessions in ^{125}Te and ^{126}Te.

E_x (keV)	E_γ (keV)	Transition	$\Delta\theta$ (mrad)
		^{125}Te	
444	408	$3/2^+ \rightarrow 3/2^+$	-36.35 ± 2.67
	444	$3/2^+ \rightarrow 1/2^+$	-29.04 ± 6.25
			$\langle -35.22 \pm 2.46 \rangle$[a]
463	428	$5/2^+ \rightarrow 3/2^+$	-10.85 ± 1.33
	463	$5/2^+ \rightarrow 1/2^+$	-13.23 ± 2.97
			$\langle -11.25 \pm 1.21 \rangle$[b]
671	636	$5/2^+ \rightarrow 3/2^+$	$+1.6 \pm 15.8$
		^{126}Te	
666	666	$2^+ \rightarrow 0^+$	-19.45 ± 0.98

[a]Average value for the 444-keV $3/2^+$ state.
[b]Average value for the 464-keV $5/2^+$ state.

The slopes $S(\theta_\gamma)$ of the angular correlations required to determine the transient-field precession angles $\Delta\theta$ for the various experimental runs are summarized in Table IV. There is considerable variation in the values of $S(\theta_\gamma)$, depending on the transition and the detection angle. As indicated in Table I, all data for which at least one pair of γ-ray detectors were placed symmetrically about the beam axis at $\pm\theta_\gamma$ were analyzed to determine the precession angles $\Delta\theta$. A variety of γ-ray detection geometries were included in the precession measurement to cover the optimal measurement conditions (near maximum slope) for each transition of interest.

Along with the states shown in Fig. 1, the decays from several weaker populated states in ^{125}Te are evident in Fig. 2. In the cases where these transitions feed into the $3/2_2^+$ and $5/2_1^+$ states, their influence has been included in the calculations of the angular correlations. Because of their low intensity, the effect on the g-factor measurement can otherwise be ignored; it is much smaller than the statistical precision of the precession measurement. This statement is based on detailed calculations. For example, the net precession of the $3/2_2^+$ 444-keV level is affected most strongly by feeding from the 1018-keV level. For changes in the g factor of the feeding state between 0.2 and 0.6 (i.e., assuming $g = 0.4 \pm 0.2$), the extracted g factor of the fed state changes by only $\pm 2\%$. Likewise, the observed precession of the $5/2_1^+$ level is influenced by feeding from the 1018- and 1029-keV levels, but the effect is again small for any reasonable values of the (unknown) g factors of the feeding states. Further discussion of the effects of feeding in transient-field g-factor measurements has been provided in Ref. [11] and references therein.

Measured precession angles are summarized in Table V. In contrast with the previous studies [10,11], the agreement between the precession angles observed via the two transitions depopulating the $3/2_2^+$ level (408 and 444 keV) is excellent, as is the agreement for the two transitions depopulating the $5/2_1^+$ level (428 and 463 keV). To calibrate the strength of the transient field, we adopt $g = +0.339(13)$ for the 2_1^+ level in ^{126}Te [11], thus obtaining $\phi = \Delta\theta/g = 57.4(3.6)$ mrad for ^{126}Te in our measurement. This result is consistent with that obtained in our similar study of the 2_1^+ states in the even Te isotopes [11]. The values of ϕ for the states in ^{125}Te shown in Table VI have been corrected for small changes in the reaction kinematics and for differences in the level lifetimes.

If one takes into account the statistical uncertainties, the agreement between the present and previous measured g factors is satisfactory. Because of the low intensity of the 671-keV line (Fig. 2) and the low anisotropy of the 636-keV line (Fig. 3), the g factor of the $5/2^+$ level at 671 keV could only be determined with poor precision. We obtained $g = -0.03(28)$, which is consistent with $g = -0.22(28)$ reported previously [10].

IV. DISCUSSION: SHELL MODEL AND WEAK-COUPLING MODEL CALCULATIONS

Shell model calculations were performed for the low-excitation positive-parity states in ^{125}Te. These calculations are similar to those reported for the Xe and Te isotopes near $N = 82$ [22]. The OXBASH code [23] was employed with the SN100PN basis, which includes proton and neutron orbits in the shell with $50 \leqslant Z, N \leqslant 82$, specifically $1g_{7/2}$, $2d_{5/2}$, $3s_{1/2}$, $1h_{11/2}$, and $2d_{3/2}$.

The single-particle energies were chosen to reproduce the single-proton states in $^{133}_{51}\mathrm{Sb}_{82}$ and the single-neutron hole states in $^{131}_{50}\mathrm{Sn}_{81}$. Surface delta interactions were used to represent the two-body residual interactions. For proton-proton interactions $A_{\pi\pi} = 0.23$ MeV, for neutron-neutron interactions $A_{\nu\nu} = 0.19$ MeV, and for proton-neutron interactions $A_{\pi\nu} = 0.25$ MeV. Because core polarization and meson-exchange currents affect the single-particle g factors, the orbital and spin g factors of both protons and neutrons were chosen to reproduce the experimental g factors of low-excitation states near $Z = 50$ and $N = 82$ that can be associated with a single-nucleon state (see Ref. [22] for details). The values adopted

TABLE VI. Measured g factors in ^{125}Te.

E_x (keV)	τ (ps)[a]	I^π	$\Delta\theta$ (mrad)	ϕ (mrad)	g factor		
					Present[b]	Ref. [10]	Ref. [11]
444	27.6	$3/2^+$	-35.2 ± 2.5	56.7 ± 3.6	$+0.620 \pm 0.058$	$+0.43 \pm 0.12$	$+0.66 \pm 0.18$
463	19.0	$5/2^+$	-11.2 ± 1.2	56.4 ± 3.6	$+0.199 \pm 0.025$	$+0.20 \pm 0.05$	$+0.34 \pm 0.09$
671	1.8	$5/2^+$	$+1.6 \pm 15.8$	56 ± 4	-0.03 ± 0.28	-0.22 ± 0.28	

[a]Mean lives from Ref. [9].
[b]$g = \Delta\theta/\phi$.

TABLE VII. Shell model results for ^{125}Te.

I^π	E_x(keV)		g factor		Dominant odd-neutron occupation
	Theory	Exp	Theory	Exp[a]	
$1/2^+$	0	0	−2.514	−1.777	$\nu s_{1/2}$
$3/2^+$	63	35	+0.557	+0.403(3)	$\nu d_{3/2}$
$3/2^+$	622	444	+0.827	+0.62(6)	$\nu s_{1/2}$
$5/2^+$	594	463	+0.200	+0.20(3)	mixed $\nu s_{1/2}$, $\nu d_{3/2}$
$5/2^+$	892	671	+0.102	−0.1(2)[b]	mixed $\nu s_{1/2}$, $\nu d_{3/2}$

[a]From Ref. [24] and present work.
[b]Weighted average of present and previous measurements; see text.

are $g_l(\pi) = 1.13$, $g_s(\pi) = 4.04 = 0.72 g_s^{\text{free}}(\pi)$, $g_l(\nu) = 0.02$, and $g_s(\nu) = -2.65 = 0.69 g_s^{\text{free}}(\nu)$.

It is not feasible to perform an unrestricted shell model calculation for ^{125}Te; therefore, protons were constrained to the $\pi 1g_{7/2}$ and $\pi 2d_{5/2}$ orbits, and neutron holes were constrained to the $\nu 3s_{1/2}$, $\nu 1h_{11/2}$, and $\nu 2d_{3/2}$ orbits (i.e., the $\nu 1g_{7/2}$ and $\nu 2d_{5/2}$ orbits were filled). Furthermore, it was required that at least six neutrons remain in the $\nu 1h_{11/2}$ orbit. Results of the calculation are compared with the experiment in Table VII.

Table VIII compares the experimental g factors in ^{125}Te with the calculated g factors of candidate weak-coupled configurations obtained by assuming $g(2^+) = 0.34$, the experimental g factor of the 2^+ level in ^{126}Te, and single neutron g factors based on the effective g_s and g_l values adopted for the shell model calculations.

Given that shell model calculations use a severely restricted basis, it is not surprising that the calculated excitation energies are all higher than the experimental values. The level order is reasonable, however, and together with the weak-coupling model calculations, the shell model results allow an identification of the dominant orbital occupation of the odd neutron in the low-lying positive-parity states in ^{125}Te.

Although there is more configuration mixing than the simple models predict, it is clear that in ^{125}Te the $1/2^+$ ground state and the first excited state at 35 keV with $I^\pi = 3/2^+$ should be associated with occupation of the $\nu 3s_{1/2}$ and $\nu 2d_{3/2}$ orbits, respectively. The $3/2_2^+$ and $5/2_1^+$ states, both near 0.45-MeV excitation energy, cannot be so readily associated with the occupation of a single neutron orbit. The shell model has a dominant occupation of the $\nu 3s_{1/2}$ orbit in the $3/2_2^+$ state and rather mixed occupation of both $\nu 3s_{1/2}$ and $\nu 2d_{3/2}$ orbits in the $5/2^+$ state. Experimentally, it is striking that $g(3/2_2^+)/g(5/2_1^+) \sim 3$. On the basis of the shell model calculations and comparisons with the g factors of the weak-coupled configurations in Table VIII, it can be inferred that this difference in the magnitude of the two g factors must stem from the occupation of the $\nu 3s_{1/2}$ orbit, which has the effect of reducing the g factor of the $5/2^+$ level while increasing that of the $3/2^+$ state.

In this context, it is of note that the excitation energies, Coulomb excitation cross sections, and relatively strong $E2$ decays to the $3/2_2^+$ and $5/2_1^+$ states make the newly identified $7/2^+$ and $9/2^+$ states at 1018 and 1029 keV, respectively, candidates for the coupling of the $s_{1/2}$ neutron to the 4^+ excitation of the core. Thus, as a generalization, the $\nu 3s_{1/2}$ orbit seems to play an important role in the states that are most strongly Coulomb excited in ^{125}Te.

TABLE VIII. g factors of weak-coupled configurations.

I_i^π	g_{exp}	Candidate configuration	g_{config}
$1/2_1^+$	−1.777	$0^+ \otimes \nu s_{1/2}$	−2.65
$3/2_1^+$	+0.403(3)	$0^+ \otimes \nu d_{3/2}$	+0.554
$3/2_2^+$	+0.62(6)	$2^+ \otimes \nu s_{1/2}$	+0.938
		$2^+ \otimes \nu d_{3/2}$	+0.383
$5/2_1^+$	+0.20(3)	$2^+ \otimes \nu s_{1/2}$	−0.258
		$2^+ \otimes \nu d_{3/2}$	+0.419

V. SUMMARY AND CONCLUSION

The g factors of the $3/2_2^+$ and $5/2_1^+$ states in ^{125}Te have been measured by the transient-field technique. The new results are consistent with previous measurements, but they are significantly more precise. From comparisons with limited-basis shell model calculations and the weak-coupling scenario, it is apparent that the lowest few positive-parity states in ^{125}Te retain features that are characteristic of the coupling of the odd neutron in the $\nu 3s_{1/2}$ and $\nu 2d_{3/2}$ orbits to the 0_1^+ and 2_1^+ excitations of the even core, despite the configurations being more mixed than the simple models predict.

The new measurements make it possible to calibrate the free-ion hyperfine interaction for Te ions recoiling in vacuum for times up to ∼30 ps, bringing us closer to a g-factor measurement by the RIV technique on the neutron-rich isotope ^{136}Te.

ACKNOWLEDGMENTS

The authors are grateful to the academic and technical staff of the Department of Nuclear Physics (Australian National University) for their assistance. Allan Harding is thanked for ongoing technical support for the Hyperfine Spectrometer. This work was supported in part by the Australian Research Council Discovery Scheme Grant No. DP0773273. MCE acknowledges support from the Australian Postgraduate Award (APA) scheme.

[1] D. C. Radford *et al.*, Phys. Rev. Lett. **88**, 222501 (2002).
[2] C. J. Barton *et al.*, Phys. Lett. **B551**, 269 (2003).
[3] J. Terasaki, J. Engel, W. Nazarewicz, and M. Stoitsov, Phys. Rev. C **66**, 054313 (2002).
[4] N. Shimizu, T. Otsuka, T. Mizusaki, and M. Honma, Phys. Rev. C **70**, 054313 (2004).
[5] B. A. Brown, N. J. Stone, J. R. Stone, I. S. Towner, and M. Hjorth-Jensen, Phys. Rev. C **71**, 044317 (2005).
[6] N. J. Stone *et al.*, Phys. Rev. Lett. **94**, 192501 (2005).
[7] A. E. Stuchbery and N. J. Stone, Phys. Rev. C **76**, 034307 (2007).
[8] D. C. Radford (private communication).
[9] J. Katakura, Nucl. Data Sheets **86**, 955 (1999).
[10] N. Benczer-Koller, G. Lenner, R. Tanczyn, A. Pakou, G. Kumbartzki, A. Piqué, D. Barker, D. Berdichevsky, and L. Zamick, Phys. Rev. C **40**, 77 (1989).
[11] A. E. Stuchbery, A. Nakamura, A. N. Wilson, P. M. Davidson, H. Watanabe, and A. I. Levon, Phys. Rev. C **76**, 034306 (2007).
[12] A. E. Stuchbery, I. Morrison, L. D. Wood, R. A. Bark, H. Yamada, and H. H. Bolotin, Nucl. Phys. **A435**, 635 (1985).
[13] E. Bezakova, A. E. Stuchbery, H. H. Bolotin, W. A. Seale, S. Kuyucak, and P. Van Isacker, Nucl. Phys. **A669**, 241 (2000).
[14] M. P. Robinson, A. E. Stuchbery, E. Bezakova, S. M. Mullins, and H. H. Bolotin, Nucl. Phys. **A647**, 175 (1999).
[15] A. E. Stuchbery, A. B. Harding, D. C. Weisser, N. R. Lobanov, and M. C. East (unpublished).
[16] A. E. Stuchbery and E. Bezakova, Aust. J. Phys. **51**, 183 (1998).
[17] J. Honzátko *et al.*, Nucl. Phys. **A645**, 331 (1999).
[18] A. E. Stuchbery, L. D. Wood, H. H. Bolotin, C. E. Doran, I. Morrison, A. P. Byrne, and G. J. Lampard, Nucl. Phys. **A486**, 374 (1988).
[19] A. E. Stuchbery, S. S. Anderssen, and H. H. Bolotin, Nucl. Phys. **A669**, 27 (2000).
[20] N. Benczer-Koller, M. Hass, and J. Sak, Annu. Rev. Nucl. Sci. **30**, 53 (1980).
[21] K.-H. Speidel, O. Kenn, and F. Nowacki, Prog. Part. Nucl. Phys. **49**, 91 (2002).
[22] G. Jakob *et al.*, Phys. Rev. C **65**, 024316 (2002).
[23] B. A. Brown, A. Etchegoyen, N. S. Godwin, W. D. M. Rae, W. A. Richter, W. E. Ormand, E. K. Warburton, J. S. Winfield, L. Zhao, and C. H. Zimmerman, Michigan State University Report No. MSU-NSCL 1289, 2004 (unpublished).
[24] N. J. Stone, At. Data Nucl. Data Tables **90**, 75 (2005).